Chapter 6

Anisotropy-based Failure for an Interphase System

(This paper is coauthored by Jianfeng Wang, Joseph E. Dove and Marte S. Gutierrez)
Dr. Joseph E. Dove is my major advisor and Dr. Marte S. Gutierrez is my co-advisor.

The ability to predict the strength of interphase systems composed of granular material in contact with natural and manufactured surfaces is a critical need in geomechanics. Previous research has focused on developing empirical and semi empirical relationships between surface profile roughness, particle size and strength. This approach does not appear to be general, and is unable to account for the surface to particle interactions at the appropriate scale. This paper presents a new failure criterion that employs the concept of anisotropy in particle to surface contact forces. A parametric study using two-dimensional discrete element method simulations of interphase systems within a standard direct interface shear test device was conducted. Particles consist of poly-disperse and mono-disperse spheres of constant median grain diameter. Surface roughness and texture complexity are varied by using profiles of regular and random asperities, and profiles of manufactured surfaces. Results indicate the magnitude and direction of average contact resultant force at the interface controls strength. A bilinear relationship, independent of particle to surface friction coefficient, exists between the principal direction of resultant contact force anisotropy and strength. Results using the proposed criterion are in good agreement with laboratory results using spheres and subrounded sand.

KEY WORDS: Anisotropy, Dilatancy, Interfaces, Failure criteria, Discrete analysis, Interphase

6.1. Introduction

An *interphase* within a geotechnical composite system is a region that consists of an inclusion surface with its asperities and a variable thickness of granular material directly adjacent to the surface. The *interface* is the boundary between the surface, with its asperities, and the particles touching the surface. For the purpose of this paper, the thickness of the granular portion of the interphase is the thickness of the shear band, which is found through numerical simulations to extend about 10 to 14 median particle diameters from the rough surface (Wang et al., 2005a). Shear displacement of the continuous material with respect to the particles is resisted by the shear strength developed by the granular material within the interphase. The interphase governs the overall behavior of a composite system and the ability to quantify this behavior is of considerable significance to civil engineering. The goal of this paper it to present a new failure criterion based on anisotropy of contact forces acting at the interface.

6.1.1. Background

A substantial body of research is available in geotechnical engineering whereby the "roughness" of natural and engineering surfaces is related to strength behavior of the mating materials (Patton 1966; Ladanyi and Archambault 1969; Barton and Choubey 1977; Ladanyi and Archambault 1980; Desai 1981; Yoshimi and Kishida 1982; Kishida and Uesugi 1987; Paikowsky 1989; Irsyam and Hryciw 1991; Hryciw and Irsyam 1993; Tejchman and Wu 1995; Ebeling et al. 1997; Day and Potts 1998; Dove and Frost 1999; Gomez 2000; Esterhuizen et al. 2001; and Dove and Jarrett 2002). Despite these important contributions, general predictive relationships that account for granular material and inclusion surface properties remain elusive. This is less of a problem for fully dilative interface systems (Dove and Jarrett 2002) that result in relatively high degree of granular material strength mobilization. However, it is a considerable problem for the majority of interphase systems that have strength mobilization somewhere between a non-dilative and a fully-dilative system. This is because mechanisms responsible for interphase strength develop at the particle to surface contacts and statistical parameters, single-value parameters, fractals and Fourier series approximations used in surface characterization have a naturally high degree of homogenization. Normalized parameters that account for the relative grain to surface geometry (Yoshimi and Kishida 1982; Kishida and Uesugi 1987) are

found useful for some surfaces. This and other parameters are useful for some systems but are generally not sufficiently robust to capture the complexity of relative geometry.

Discrete methods of investigation have provided important details regarding geotechnical interface behavior. Discrete simulations and experiments provide realistic insight into fundamental mechanisms of interphase behavior. For example, Paikowsky and Xi 1997 performed an extensive laboratory study and discrete modeling on both the micro and macro mechanical interfacial behavior using photoelastic methods. Numerical simulations by Jensen et al. 1999, Claquin and Emeriault 2001 and Frost et al. 2002 provide insight into surface geometry and hardness effects on interface behavior.

6.1.2. Primary work of the current paper

This paper presents a failure criterion that relates the principal direction of surface normal distribution (θ_a) to interphase strength. This criterion is rooted in the fundamental source of particulate-solid interphase strength wherein the grains in direct contact with the inclusion surface control the degree of mobilized interphase shear resistance. The proposed failure criterion accounts for the presence of an inclusion surface with any degree of roughness. While developed for spherical particles it is believed the methodology is general for any particle shape due to inclusion of particle rolling resistance.

6.2. Experimental Methods

A parametric numerical study was conducted using the two-dimensional discrete element program PFC2D, Version 3.0 (Itasca Consultants, Inc.). A direct interface shear device model was developed (See Chapter 2, 3 and 5) and validated against laboratory data (Dove and Jarrett 2002; Johnson 2000). These laboratory data are used to test the proposed failure criteria.

A direct shear box model was also developed to determine the stress-displacement behavior and peak strength of the granular assemblage (See Chapter 2 and 4). With strength data from similar simulations it is possible to express the results in terms of interface efficiency.

6.2.1. Granular material

Granular materials include both mono-disperse (uniform) and poly-disperse (well-graded) particle size distributions. Particles were modeled as spheres for calculation of contact stress. The maximum and minimum particle diameters (D_{max}, D_{min}) are 0.735 mm and 0.665 mm respectively, for the mono-disperse material, and 1.05 mm and 0.35 mm respectively, for the poly-disperse material. The median particle diameter (D_{50}) is held constant at 0.7 mm so that the influence of gradation can be isolated. Grain to surface friction coefficients ($\tan\phi_\mu$) were 0.05, 0.2 and 0.5.

6.2.2. Parametric study

Five groups of numerical experiments were conducted. Two-dimensional surface profiles were created both analytically and by profiling construction materials. Profiles with triangular asperities of equal size were used in Groups 1, 2 and 3 with asperity height (R_t), asperity width (S_w) and spacing between asperities (S_r) varied in each group, respectively [(Figure 6.1(a)]. Table 6.1 provides the ranges of variables and constant values in these experiments. All asperity sizes are normalized with respect to D_{50}.

Table 6.1. Variables and Constants for Experimental Groups 1, 2 and 3.

			Constant Values		
Group	Variable	Values of Variable	R_t/D_{50}	S_r/D_{50}	S_w/D_{50}
1	R_t/D_{50}	0.1, 0.2, 0.5, 1, 1.2, 1.5, 2, 3, 5	Varied	0	2
2	S_r/D_{50}	0.2, 0.5, 1, 2, 3, 5, 8, 10	1	Varied	2
3	S_w/D_{50}	0.2, 0.5, 1, 2, 3, 4, 5, 10	1	0	Varied

Irregular asperities were randomly generated in Group 4 to investigate how profile complexity influences interphase behavior. These profiles are described by the parameters asperity unit (A_u), asperity ratio (A_r) and maximum accumulated asperity height (R_{tmax}) as shown on Figure 6.1(b). A_u is the unit length of the projection of any linear asperity segment in the horizontal direction. Asperity ratio is the ratio of the unit length of a projection of any linear asperity segment in the vertical direction to that in the horizontal direction. The maximum accumulated asperity height is the prescribed maximum elevation difference between the peak

and the valley over the whole surface. Asperity unit and maximum accumulated asperity height are normalized with respect to median particle diameter.

A random number multiplier is applied to the unit segment length in both horizontal and vertical directions using the values of A_u, and A_r as starting values. Control of profile geometry is through assigning different values to the above three parameters. Parameter values used in the seven numerical experiments of Group 4 are provided in Table 6.2.

Table 6.2. Values of A_u, A_r and R_{tmax} used in Experimental Group 4.

Variable	Numerical Experiment						
	A	B	C	D	E	F	G
A_u/D_{50}	1	2	2	4	2	4	4
A_r	1	1	0.5	2	0.25	0.25	4
R_{tmax}/D_{50}	2	2	2	4	1	2	4

Profiles in Group 5 were made with a stylus profilometer from natural and manufactured surfaces. These include three coextruded geomembranes, wood, stone and concrete. These profiles have a richer frequency content than those in Groups 1 through 4 due to the more complex texture patterns [Figure 6.1(c)].

6.2.3. Global model parameters

The Hertz-Mindlin contact model was implemented in the simulations. A particle rolling resistance model (See Chapter 2) was also applied at both particle-particle contacts and particle-boundary contacts. Physical constants used in the simulations include: Particle density 2,650 kg/m^3, shear modulus 29 GPa and Poisson's ratio of the particles 0.3. Critical normal and shear viscous damping coefficients are set equal to 1.0. A time step 5.0×10^{-5} sec was used. Interparticle and particle to boundary friction coefficients were 0.5 and 0.9, respectively.

6.3. Representation of Discrete Data

Continuum mechanics methods are used to place the discrete information into a framework for analysis. This framework is based on determining anisotropy of fabric and

contact forces in the assemblage using two-dimensional, second order density distribution tensors defined by Rothenburg 1980 and Bathurst and Rothenburg 1990, and described in Chapter 4 and 5. Anisotropy refers to the deviation of contact and contact force orientation from the isotropic state.

These distributions are approximated using Fourier series expressions (Bathurst and Rothenburg 1990). Principal directions of average contact resultant force anisotropy (θ_r) and contact normal force anisotropy (θ_n) are determined from the Fourier approximations. These principal directions correspond to the eigenvectors of the stress tensors and therefore correspond to principal directions. θ_r and θ_n are not direct measures of the inclusion surface roughness but result from actual mechanical interaction between the surface asperities and granular media. They implicitly account for the statistical nature of the surface roughness relative to the particle size. Detailed discussion of the analysis methods is presented in Chapter 5.

6.4. Results

6.4.1. Mechanism for shear strength mobilized inside the interphase

An understanding the mechanism by which contact forces are transmitted from the interface into the soil mass is required before a failure criterion can be developed. Figure 6.2 illustrates examples of contact force networks recorded at peak state from one regular saw tooth surface and one coextruded HDPE geomembrane surface. Majmudar and Behringer 2005 present details of contact force transmission in granular material. The individual figures have slightly different scales therefore thicknesses of force chains are not comparable. From these plots it is possible to visualize how the orientation of major force chains changes as they extend into the matrix soil from the surface. Figure 6.2(a) is a 45-degree asperity slope saw tooth profile. The contact force chains are perpendicular to the asperity surface and then curve toward horizontal only slightly as they extend into the interphase region. These extended force chains engage a large number of adjacent particles that force shear failure to occur inside the interphase soil. In a continuum sense, the surface is able to develop anisotropy of fabric and contact forces inside the interphase region that are similar to those occurring inside the granular media subject to direct shear. The shear band is fairly thick and the stress ratio is high for this combination of relative particle to surface roughness.

From Figure 6.2(b) it is seen that force chains preferentially develop on the larger asperities, or asperities that are spaced wider than the grain diameter. Many of the contact orientations are vertical, or nearly so. Chains curve and become closer to horizontal as they extend into the interphase region. This is because the force chains at the surface are too steep to involve a large number of particles above the surface in intense shearing; therefore horizontal forces applied during shear influence their direction. Smaller degrees of fabric and contact force anisotropies are developed in the interphase region. Particle sliding also occurs along the surface, leading to a very thin shear zone just above the surface.

The mechanism described above is illustrated by sampling two different regions within the simulated interface shear box and computing the corresponding stress ratio. Figure 6.3 shows the variation in average stress ratio measured inside the interphase region from all simulations using poly-disperse material with θ_n and θ_r measured at the surface asperities. The "average stress ratio" is computed using the average stress tensor (Rothenburg and Selvadurai 1981; Christoffersen et al. 1981) within a rectangle that extends into the interphase a distance of 14 mm from the interface, with length corresponding to the length of the rough surface. In contrast, "stress ratio" is the ratio of the sum of horizontal and vertical components of contact forces due to the particles touching the asperities and is approximately equal to the direct shear friction angle [Figure 6.4(a)]. The bilinear relationships developed are similar in form between the two locations. The magnitude of the average stress ratio measured in the 14 mm high sampling region near the interface is slightly lower than the stress ratio computed from force summation at the surface asperities. This is because stresses developed at the surface diminish in the interphase region away from the surface. It must be noted, however, that inside the interphase, stress ratio is determined by the combined effects of fabric and contact force anisotropies (See Chapter 5), and is also affected by the horizontal stress σ_{xx}, which is not applicable when summing forces at the asperities. θ_n or θ_r within the granular assemblage coincides with the principal stress direction throughout the shear process [Figure 6.4(b)].

These results indicate that the same mechanism of force transmission resulting from the contacts between particles operates at the interface and within the interphase region. Figure 6.3 indicates that this mechanism, and its effect on mobilized shear strength, can be quantified through the principal directions the contact force distributions at the surface.

6.4.2. *Correlation based on* R_n

In the literature, there are numerous ways to characterize surfaces based on parameters computed from the statistics of a surface profile. Much work has been done to relate those statistical parameters to the interface strength behavior. Kishida and Uesugi 1987 proposed a normalized roughness parameter R_n for steel surfaces, which is defined as:

$$R_n = \frac{R_{t,ave}(L = D_\alpha)}{D_\alpha}, \tag{6-1}$$

where $R_{t,ave}$ is the average value of the maximum asperity height over a series of assessment lengths, L, that are equal to a characteristic grain diameter D_α. Kishida and Uesugi 1987 let D_α equal D_{50}, the median grain diameter, and correlated $R_{n(D_{50})}$ with the strength of sand-steel interfaces. Although they obtained a linear correlation between $R_{n(D_{50})}$ and the peak friction angle, the results are only limited to the steel surfaces which are fairly smooth and have very low $R_{n(D_{50})}$ values. For other dilative surfaces with greater grain-surface roughness and wider range of $R_{n(D_{50})}$ values, the use of $R_{n(D_{50})}$ as a unique parameter becomes problematic.

This problem is addressed in Figure 6.5. Values of $R_{n(D_{50})}$ are calculated for all the surfaces tested and plotted against the peak interface strength values. But the method used here is a bit different from the original one in that $R_{n(D_{50})}$ is not calculated based on the actual surface profile. Instead, it is calculated using the profile obtained by tracing the centroid of a particle with median particle diameter when it rolls across the entire surface. Correspondingly, the parameter is denoted as $R_{nc(D_{50})}$. This method is first used by DeJong et al. 2002 to measure the relative surface roughness. They conclude that $R_{nc(D_{50})}$ better reflects the relative grain-surface roughness. For nondilative surfaces such as steel surfaces, there is little difference between $R_{n(D_{50})}$ and $R_{nc(D_{50})}$ but for highly dilative surfaces, especially irregular surfaces, the difference could be large. Figure 6.5 shows that data from Kishida and Uesugi agree with our simulation data in terms of strength ratio but have a steeper slope and higher upper limit in terms of efficiency. It is probably due to the irregular shape of sand grains as opposed to the spherical particle shape used in the current study. But these data are only limited in a low $R_{nc(D_{50})}$ range.

Our simulation data cover a much broader range of grain-surface roughness and include a wide variety of surfaces. However, it can be seen that $R_{nc(D_{50})}$ does not give a unique correlation with peak interface strength, with data from discontinuous surfaces (Group 2), irregular surfaces (Group 4) and real surfaces (Group 5) deviating significantly from the linear relation. This is mainly due to the inclusion of the flat portions of the surface in the $R_{nc(D_{50})}$ calculation that does not contribute much to the total interface strength ratio.

6.4.3. Failure criterion for interphase systems

A failure criterion relating the interface strength to easily measured properties of granular material and inclusion surfaces can be established using Figure 6.3 and the principle of contact anisotropy. θ_n and θ_r are derived from the discrete simulations and are not easily determined from laboratory tests. Therefore a parameter that can be determined from surface profiles and a standard grain size distribution is needed for practical use. The principal direction of the surface normal distribution, θ_a provides a means to easily determine θ_r.

Polar distributions of surface normals of four selected surfaces are shown on Figure 6.6. The distributions are based on the particle centroid trace surface profile (DeJong et al. 2002) obtained using a particle with median diameter of 0.7 mm. Relative motion between the grains and the surface during shear displacement results in contacts on portions of the asperities that oppose shear along the interface. Accordingly, the surface normal distribution located in the first quadrant with respect to the surface is neglected. The principal direction, θ_a, is based on the Fourier approximation to the normals occurring in the second quadrant with respect to the surface. Principal directions are indicated by the arrows in Figure 6.6.

Figure 6.7 presents the relationship between peak stress ratio measured at the interface and θ_a for all five simulation groups. In Figure 6.7(a), θ_a is calculated using all contact normals, including the flat segments with normal angle equal to 90 degrees from horizontal. Significant deviation of data from Groups 2 and 5 is observed. The cause of the scatter at stress ratios less than the maximum is that these profiles include high percentage of flat portions with vertical normals as shown on the polar distributions of Figure 6.6(c) and 6.6(d). However, these contacts do not contribute in a significant way to the total strength measured along the surface because particles are either “trapped” within the asperities or undergo sliding along the smooth surface.

Exclusion of these horizontal sections of the profile leads to the correlation shown in Figure 6.7(b), where θ_a is calculated using surface normals with normal angle greater than 92 degrees from horizontal. Distinct bilinear relationships are observed with interface strength ratio in the lower interface friction cases (0.05 and 0.2). Greatest variation is observed in the high interface friction case (0.5). In Figures 6.7(b), 6.7(d), and 6.7(f), it is observed that profiles with horizontal spacing between asperities (Group 2) have θ_a of approximately 42 degrees even though the stress ratio varies slightly. This indicates that surfaces with regular discontinuous asperity spacing require additional consideration. Such surfaces can result from machining of metals and forming of concrete.

Figure 6.8 shows correlations between θ_a and θ_r for various interface friction cases. Except for the profiles with horizontal segments (Group 2) a bilinear correlation exists between θ_a and θ_r. It can be seen that when $\theta_a \leq 40$ degrees, the slope of the linear portion decreases as interface friction coefficient increases. The same linear equation applies for all interface friction cases when $\theta_a > 40$ degrees [Figure 6.8(d)]. The vertical axis intercept is approximately equal to ϕ_μ. This indicates that for a given surface with a known interface friction coefficient, θ_r can be determined from θ_a. Figure 6.9 provides additional correlations between θ_a and θ_r/θ_a for surfaces with horizontal spaces between asperities and a range of asperity slopes.

6.4.4. Use of the failure criterion

Peak efficiency or strength ratio for interphase systems composed of materials similar to those used herein can be predicted using the proposed failure criterion. First, θ_a is determined from the profile data using the centroid trace methodology based on median grain diameter. A computer program to determine θ_a was developed that uses surface profile and median grain diameter data as inputs. It is available from the authors. The program computes the centroid trace profile, the distribution of surface normals, arithmetic average asperity slope of asperities and the value of θ_a. It is recommended at this time to use unfiltered, centerline corrected profiles of a surface. Filtered profiles can be used depending on the surface and project requirements.

For the majority of construction material profiles, θ_a is computed using surface normals greater than 92 degrees. Then, θ_r is estimated from the correlation between θ_a and θ_r shown on

Figure 6.8(d). However, for surfaces that have regular horizontal spacing between asperities (constant S_r in Figure 6.1), θ_a is computed using surface normals greater than or equal to 90 degrees. Then Figure 6.9 is used to determine θ_r using the principal direction ratio (θ_r / θ_a). Finally, peak efficiency is estimated using the relationship shown in Figure 6.10(a). The value of asperity slope used to select a particular curve in Figure 6.9 is the arithmetic average slope of the individual asperities without the horizontal segments included.

6.4.5. Criterion based on efficiency parameter

Interface strength is often written in terms of efficiency, defined as $E = \tan\delta / \tan\phi$ where $\tan\delta$ is the effective stress interface strength parameter and $\tan\phi$ is the effective stress friction angle of the granular media alone. Figure 6.10(a) shows the relationship between peak efficiency and θ_r for all numerical experiments grouped by particle to surface friction coefficient. A distinct bilinear relationship is formed by the data. The region where θ_r is greater than about 30 degrees from vertical displays variation in peak efficiencies. This is due to inclusion of the full range of surfaces and ϕ_μ values used in this study. Not all surfaces will cause full granular material strength mobilization, which agrees with laboratory data. Within each group of surfaces, however, the variation in this region is relatively small.

6.4.6. Verification of failure criterion

Verification of the failure criterion based on θ_a is performed using laboratory interface shear test data for 0.7 mm glass beads, 0.5 mm glass beads and Ottawa 20/30 sand. Figure 6.10(b), 6.10(c) and 6.10(d) show the comparison between the simulation data and laboratory data. The surfaces used in the laboratory tests and simulations all have regular triangular asperities [Figure 6.1(a)] of the same particle to surface geometry. Root spacing, height and width is constant for each individual surface. Laboratory test surfaces were constructed of aluminum.

In Figure 6.10(b), the peak interface strength ratios of 0.7 mm glass beads measured in the laboratory are plotted against θ_a computed from profiles of the individual surfaces. It can be seen that the laboratory data and simulation data are in good agreement in terms of peak strength

ratio. The simulation data cover a much broader range of relative particle to surface geometry than can be accommodated in laboratory equipment therefore there are no laboratory data for θ_a greater than 40 degrees.

For glass bead and Ottawa sand, respectively, the particle to surface friction coefficient is about 0.1 and 0.2 for many surface materials (Dove et al. 2006). Figures 6.10(c) and 6.10(d) show the agreement between the predicted and measured peak efficiency values for glass beads and Ottawa sand. The maximum difference between the predicted and measured interface friction angles are less than 4 degrees. For 0.7 mm glass bead and Ottawa 20/30 sand, the differences are less than 1 degree, and 1 to 2 degrees for 0.5 mm glass bead. Tests results for non-dilative systems (θ_a = 0) of aluminum surface, glass beads and Ottawa sand are shown on Figures 6.10(b) and 6.10(c). These values agree with the simulations (ϕ_μ= 0.1 glass beads and 0.2 Ottawa sand).

6.5. Conclusions

This paper examines the effects of relative particle-surface geometry on the strength behavior of an interphase system composed of spherical granular particles in contact with natural or manufactured inclusion surfaces. Results indicate the magnitude and direction of the average contact resultant force controls interface strength behavior. A bilinear relationship independent of particle-surface friction coefficient exists between θ_r and the mobilized interface strength. A similar relationship holds for θ_n that is a function of particle-surface friction coefficient. Full mobilization of the granular material strength occurs when θ_r exceeds approximately 30 degrees.

A new, practical failure criterion is developed based on θ_a determined from centroid trace profiles at the median particle diameter. Good agreement with the results of laboratory interface shear test data is observed and it appears valid for rounded and sub-rounded particles. For the extreme case of profiles with constant S_r, additional correlations are provided that extend the range of surfaces that can be used.

Acknowledgements

This material is based upon work supported by the National Science Foundation under Grant No. CMS-0200949. Any opinions, findings, and conclusions or recommendations expressed in this material are those of the authors and do not necessarily reflect the views of the National Science Foundation.

Notation

The following symbols are used in this paper:

A_u = asperity unit

A_r = asperity ratio

D_{50} = median particle diameter (mm)

D_{max} = maximum particle diameter (mm)

D_{min} = minimum particle diameter (mm)

D_α = characteristic grain diameter (mm)

E = efficiency parameter

L = assessment length (mm)

R_n = normalized roughness parameter

$R_{n(D50)}$ = normalized roughness parameter

$R_{nc(D50)}$ = normalized roughness parameter based on median particle diameter particle centroid trace profile

R_t = asperity height (mm)

R_{tave} = average value of maximum asperity height over a series of assessment lengths, L (mm)

R_{tmax} = maximum accumulated asperity height (mm)

S_r = spacing between asperities (mm)

S_w = asperity width (mm)

δ = effective stress interface friction angle (degrees)

ϕ = effective stress friction angle of granular media (degrees)

ϕ_μ = particle-surface friction angle (degrees)

θ_a = principal direction of surface normal distribution (degrees)

θ_n = principal direction of average contact normal force anisotropy (degrees)

θ_r = principal direction of average contact resultant force anisotropy (degrees)

σ_{xx} = horizontal stress (kPa)

References

Bathurst, R.J., and Rothenburg, L (1990), "Observation on Stress-Force-Fabric Relationships in Idealized Granular Materials," Mechanics of Materials, 9, 65-80.

Christoffersen, J., Mehrabadi, M.M. and Nemat-Nasser, S (1981), "A Micro-mechanical Description of Granular Material Behavior," J. Appl. Mech, 48, ASME, 339-344.

Claquin, C., and Emeriault, F (2001), "Interface Behavior of Granular Materials: Discrete Numerical Simulation and Statistical Homogenization," Powders & Grains 2001, Kishino, ed., Swets & Zeitlinger, Lisse, 323-326.

Day, R.A., and Potts, D.M (1998), "The Effect of Interface Properties on Retaining Wall Behavior," Int. J. Num. Anal. Meth. In Geomech., 22, 1021-1033.

DeJong, J.T., Frost, J.D., and Saussus, D.R (2002), "Measurement of Relative Surface Roughness at Particulate-Continuum Interfaces," J. Testing and Eval., 30(1), 8-19.

Desai, C.S (1981), "Behavior of Interfaces Between Structural and Geologic Media," Proc. Intern. Conf. On Recent Adv. In Geot. Earthquake Eng. U. Missouri at Rolla, St. Louis, 619-638.

Dove, J.E., Bent, D.D., Wang, J., and Gao, B (2006), "Particle-scale Interaction of Non-dilative Interface Systems," Geotextiles and Geomembranes.

Dove, J.E., and Jarrett, J.B (2002), "Behavior of Dilative Sand Interface in a Geotribology Framework," Journal of Geotechnical and Geoenvironmental Engineering, 128(1), 25-37.

Dove, J.E., and Frost, J.D (1999), "Peak Interface Friction Behavior of Smooth Geomembrane-Particle Interfaces," J. Geotechnical Eng., 125(7), 544-555.

Ebling, R.M., Peters, J.F., and Mosher, R.L (1997), "The Role of Non-linear Deformation Analysis in the Design of a Reinforced Soil Berm at Red River U-Frame Lock No. 1," Int. J. Num. and Anal. Meth. In Geomech, Vol. 21, 753-787.

Esterhuizen, J.J.B., Filz, G.M., and Duncan, J.M (2001), "Constitutive Behavior of Geosynthetic Interfaces," Journal of Geotechnical and Geoenvironmental Engineering, 127(10), 834-840.

Frost, J.D., DeJong, J.T., and Recalde, M (2002), "Shear Failure Behavior of Granular-Continuum Interfaces," Eng. Fracture Mech., 69, 2029-2048.

Hryciw, R.D., and Irsyam, M (1993), "Behavior of Sand Particles Around Rigid Ribbed Inclusions During Shear," Soils and Foundations, 33(3), 1-13.

Irsyam, M., and Hryciw, R.D (1991), "Frictional and Passive Resistance in Soil Reinforced by Plane Ribbed Inclusions," Géotechnique, 41(4), 485-498.

Gomez, J.E (2000), "Development of an Extended Hyperbolic Model for Concrete to Soil Interfaces," Ph.D. dissertation, Virginia Tech, Blacksburg, VA, 248p.

Jensen, R.P., Bosscher, P.J., Plesha, M.E., and Edil, T.B (1999), "DEM Simulation of Granular Media --- Structure Interface: Effects of Structure Roughness and Particle Shape," International Journal for Numerical and Analytical Methods, 23, 531-547.

Johnson, M.L (2000), "Characterization of Geotechnical Surfaces by Stylus Profilometry," Master of Science Thesis, Georgia Institute of Technology, 504 p.

Kishida, H., and Uesugi, M (1987), "Tests of Interface between Sand and Steel in the Simple Shear Apparatus," Géotechnique, 37(1), 45-52.

Ladanyi, B., and Archambault, G (1980), "Direct and Indirect Determination of Shear Strength of Rock Mass," Soc. Mining Eng. Annual Meeting, Las Vegas, Nevada, February 15.

Landanyi, B., and Archambault, G (1969), "Simulation of Shear Behavior of a Jointed Rock Mass," Proceeding of Eleventh Symposium of Rock Mechanics, Berkeley, California, 105-125.

Majmudar T. S., and Behringer R. P (2005), "Contact Force Measurements and Stress-induced Anisotropy in Granular Materials," Nature, 435, 1079.

Paikowsky, S.G (1989), "A Static Evaluation of Soil Plug Behavior with Applications to the Pile Plugging Problem," D. Sc. Dissertation, MIT, Cambridge, MA.

Paikowsky, S.G., and Xi, F (1997), "Photoelastic Quantitative Study of the Behavior of Discrete Materials with Application to the Problem of Interfacial Friction," Research Report, Air Force Office of Scientific Research, Research Grant F49620-93-0267.

Patton, F.D (1966), "Multiple Modes of Shear Failure in Rock," Proceeding of First Congress of International Society of Rock Mechanics, Lisbon, 1, 509-513.

Rothenburg, L (1980), "Micromechanics of Idealized Granular System," Ph.D. Dissertation, Carleton University, Ottawa, Ontario, Canada.

Rothenburg, L., and Selvadurai, A.P.S (1981), "A Micromechanical Definition of the Cauchy Stress Tensor for Particulate Media," Procs. Int. Symp. on the Mechanical Behavior of

Structured Media, (ed Selvadurai), Ottawa, Part B, 469-486.

Tejchman, J., and Wu, W (1995) "Experimental and Numerical Study of Sand-Steel Interfaces," Int. J. Num. and Anal. Meth. In Geomech., Vol. 19, 513-536.

Uesugi, M., and Kishida, H (1986), "Influential Factors of Friction between Steel and Dry Sands," Soils and Foundations, 26(2), 33-46.

Uesugi, M., and Kishida, H (1986), "Frictional Resistance at Yield between Dry Sand and Mild Steel," Soils and Foundations, 26(4), 139-149.

Uesugi, M., and Kishida, H., and Tsubakihara, Y (1988), "Behavior of Sand Particles in Sand-Steel Friction," Soils and Foundations, 28(1), 107-118.

Wang, J.F., Dove, J.E., Gutierrez, M.S., and Corton, J.D (2005), "Shear Deformation in the Interphase Region," Powders and Grains 2005 (R. Garcia-Rojo, H.J. Herrmann, S. McNamara, Eds), Stuttgart, Germany, 747-750.

Wang, J.F., Gutierrez, M.S., and Dove, J.E (2005), "Strain Localization in an Idealized Interphase System," Proc. 2005 Joint ASME/ASCE/SES Conf. Mech. Mat., Baton Rouge, Louisiana.

Wang, J.F., Gutierrez, M.S., and Dove, J.E (2004), "Effect of Particle Rolling Resistance on Interface Shear Behavior," Proceedings 17th ASCE Engineering Mechanics Conference, Newark, Delaware, 56-63.

Yoshimi, Y., and Kishida, T (1982), "A Ring Torsion Apparatus for Evaluating Friction Between Soil and Metal Surfaces," Geot. Testing J., Vol. 4, 145-152.

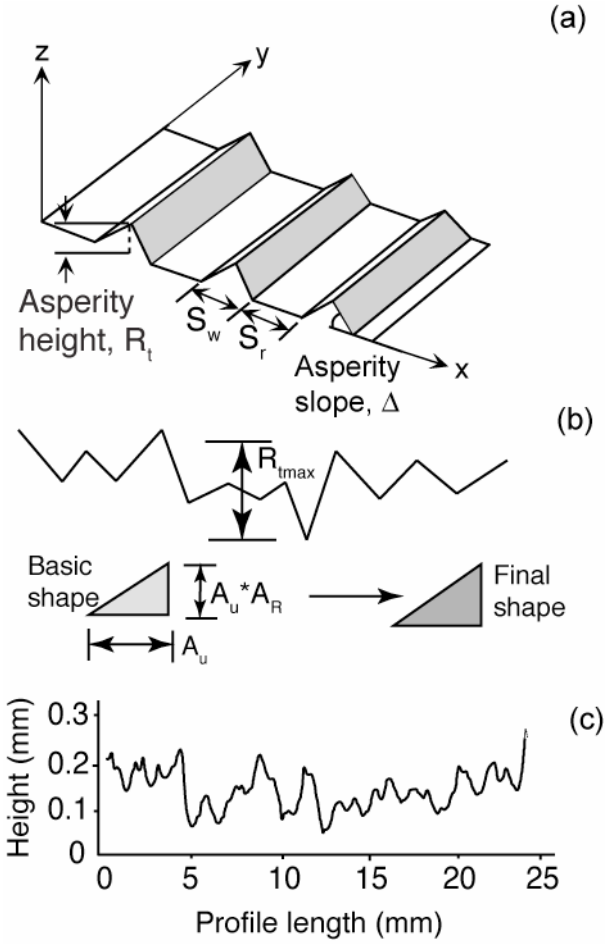

Figure 6.1. Surface geometry used in numerical experiments: (a) Groups 1, 2 and 3; (b) Group 4, Note extreme roughness of surface; (c) Example profile of concrete surface used in simulations.

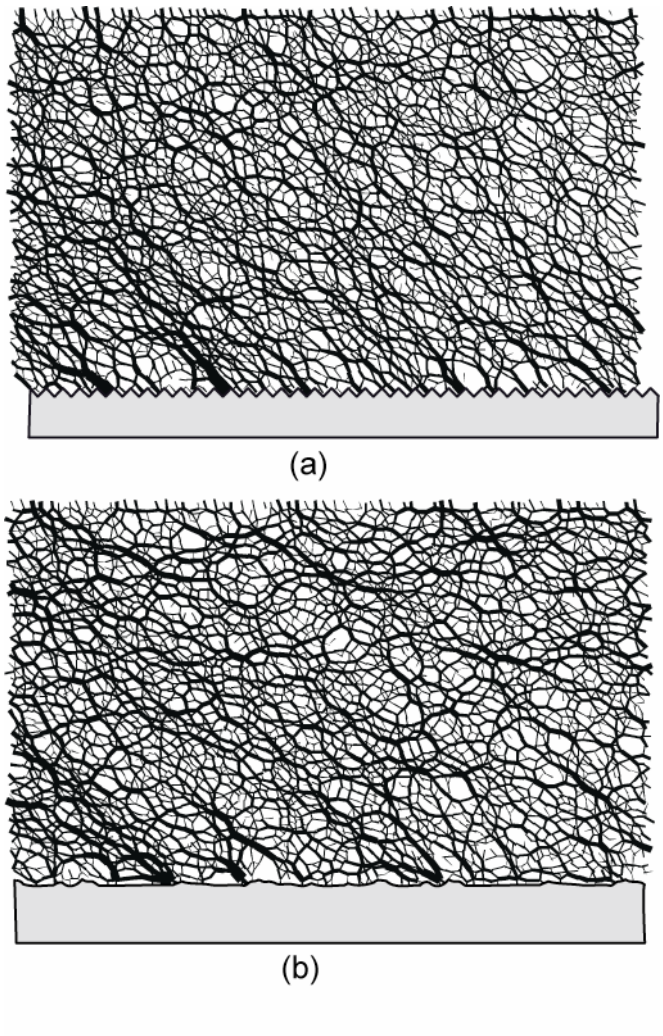

Figure 6.2. Contact force network inside the simulated interface shear device: (a) 45-degree asperity slope with R_t/D_{50} = 1.0, Group 1; (b) Coextruded geomembrane. Figures are at slightly different scales, therefore thicknesses of force chains are not comparable.

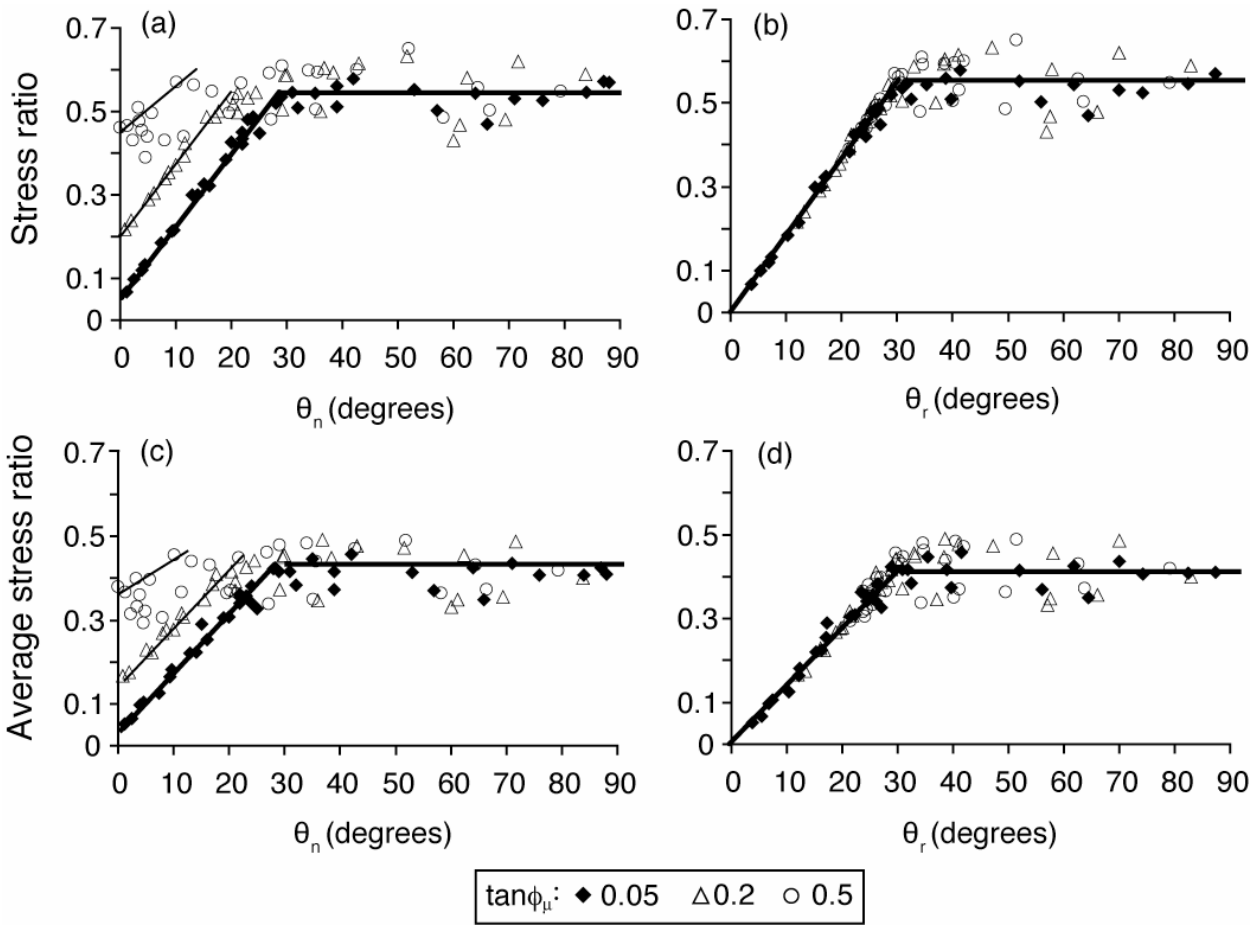

Figure 6.3. Relationship between the peak stress ratio measured at the surface and principal directions of average contact normal force (θ_n) and resultant force anisotropy (θ_r) along the surface (a) and (b). Same relationships for average stress ratio measured in the sampling region (c) and (d).

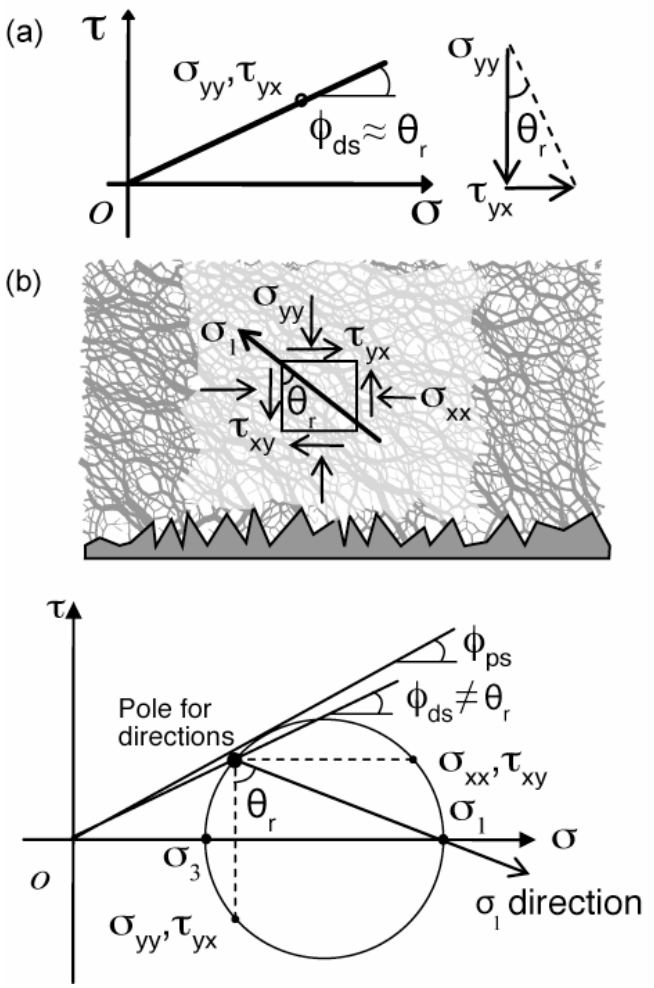

Figure 6.4. Physical meaning of θ_r at the surface and in the granular assemblage: (a) θ_r measured at the surface is the resultant angle from the sum of the normal and shear forces acting on the asperities; (b) In the interphase, θ_r corresponds to the orientation of the major principal stress.

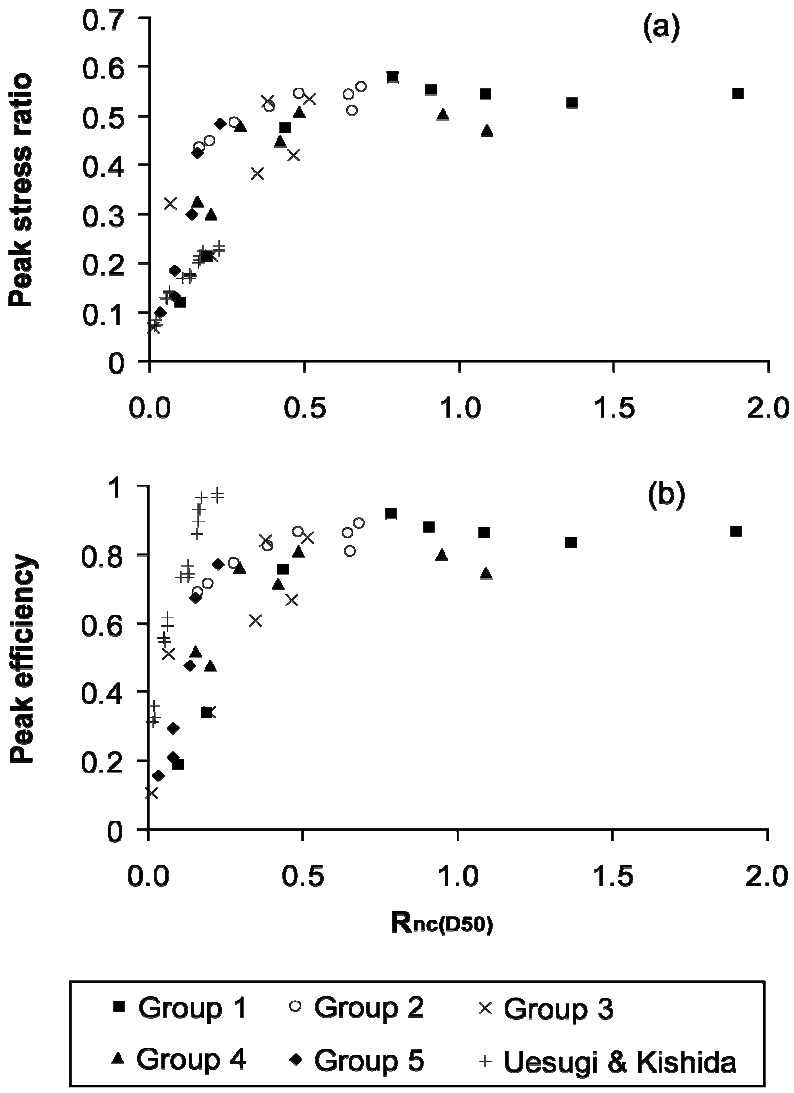

Figure 6.5. Simulation and experiment data correlating peak interface stress ratio and peak efficiency with $R_{nc(D_{50})}$. Simulation data are based on well graded material and interface friction coefficient is 0.05.

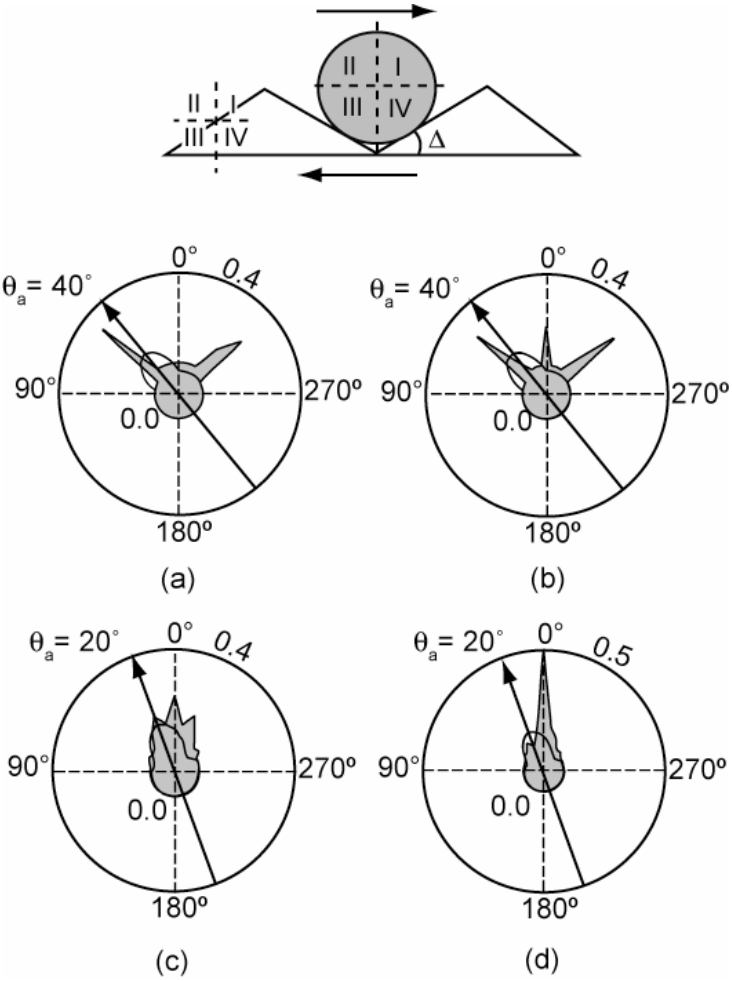

Figure 6.6. Density distributions of surface normals based on profile of particle centroid trace: (a) R_t/D_{50} = 1.0, Group 1; (b) S_r/D_{50} = 1.0, Group 2; (c) Experiment C, Group 4; (d) Geomembrane surface, Group 5. Inset figure is a key sketch of quadrant locations.

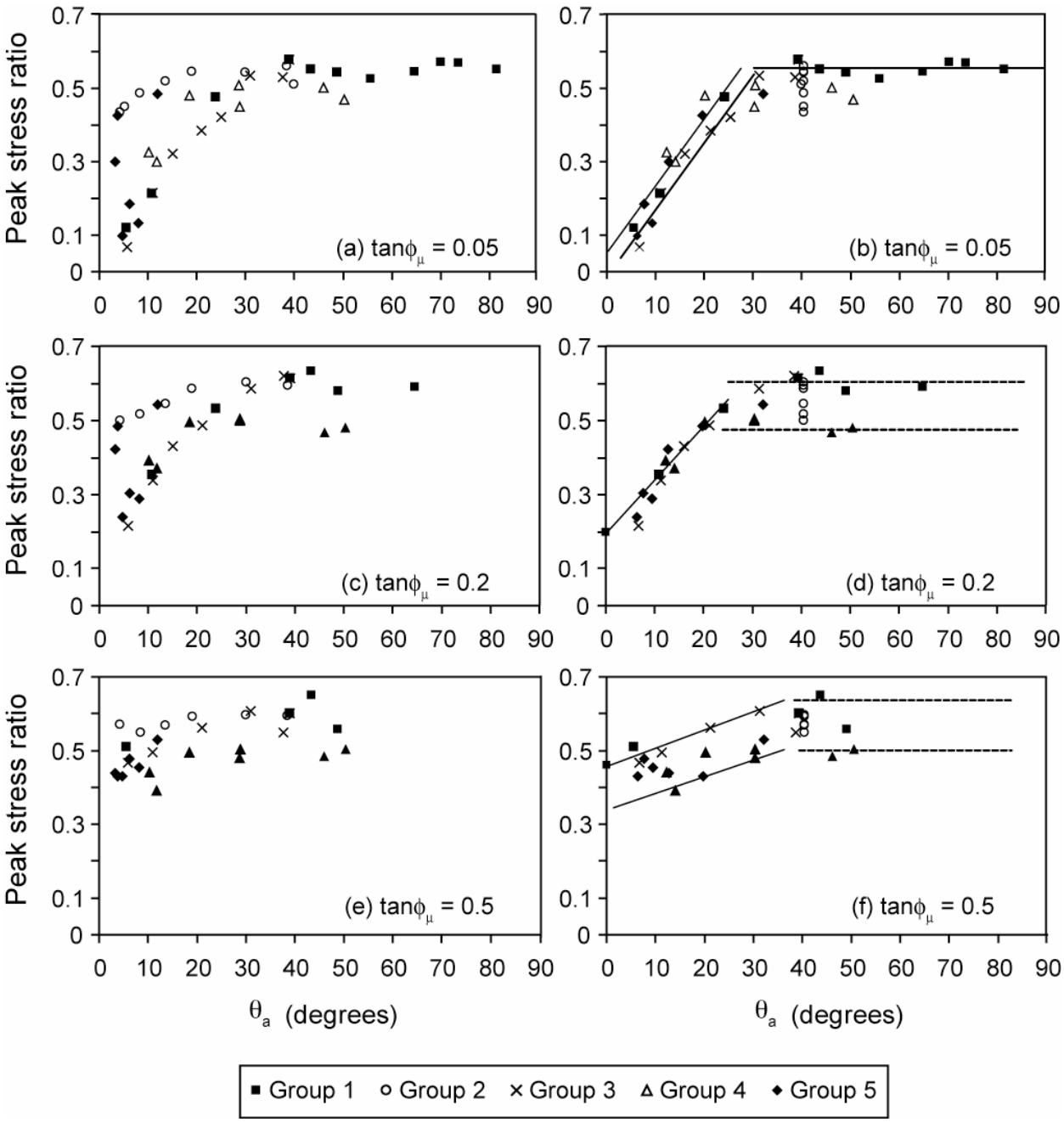

Figure 6.7. Peak stress ratio variation with principal direction of surface normal distribution (θ_a). Data are based on well-graded material. All surface normals included (a), (c) and (e). Normals less than 92 degrees filtered from the average (b), (d) and (f).

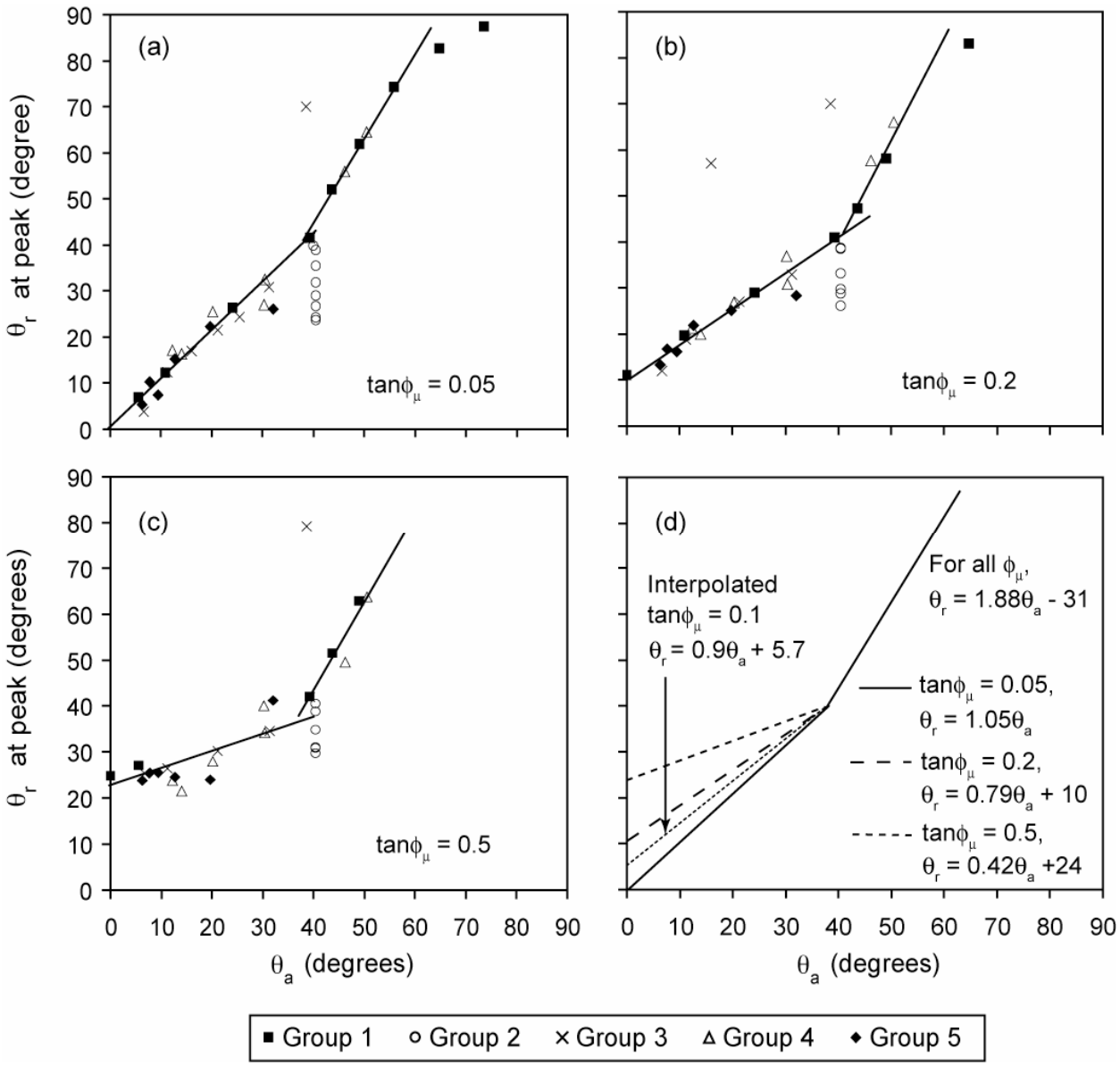

Figure 6.8. Correlations between θ_a and θ_r measured at the asperities at peak state for various particle to surface friction coefficients. Data are for well-graded material.

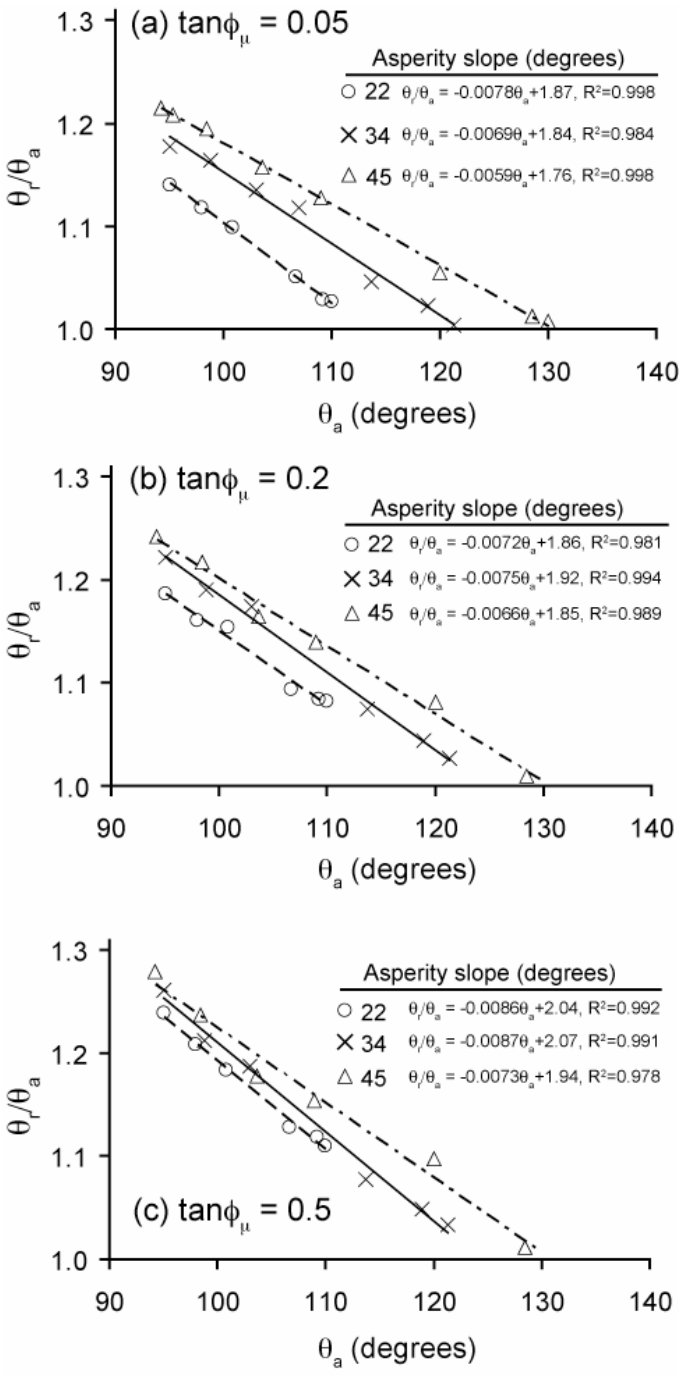

Figure 6.9. Correlation to determine θ_r from computed θ_a value for surfaces with high proportion of horizontal segments. θ_a is calculated based on surface normals with normal angle ≥ 90 degrees from horizontal; Note: θ_a on horizontal axis is referenced counterclockwise from the horizontal in this figure.

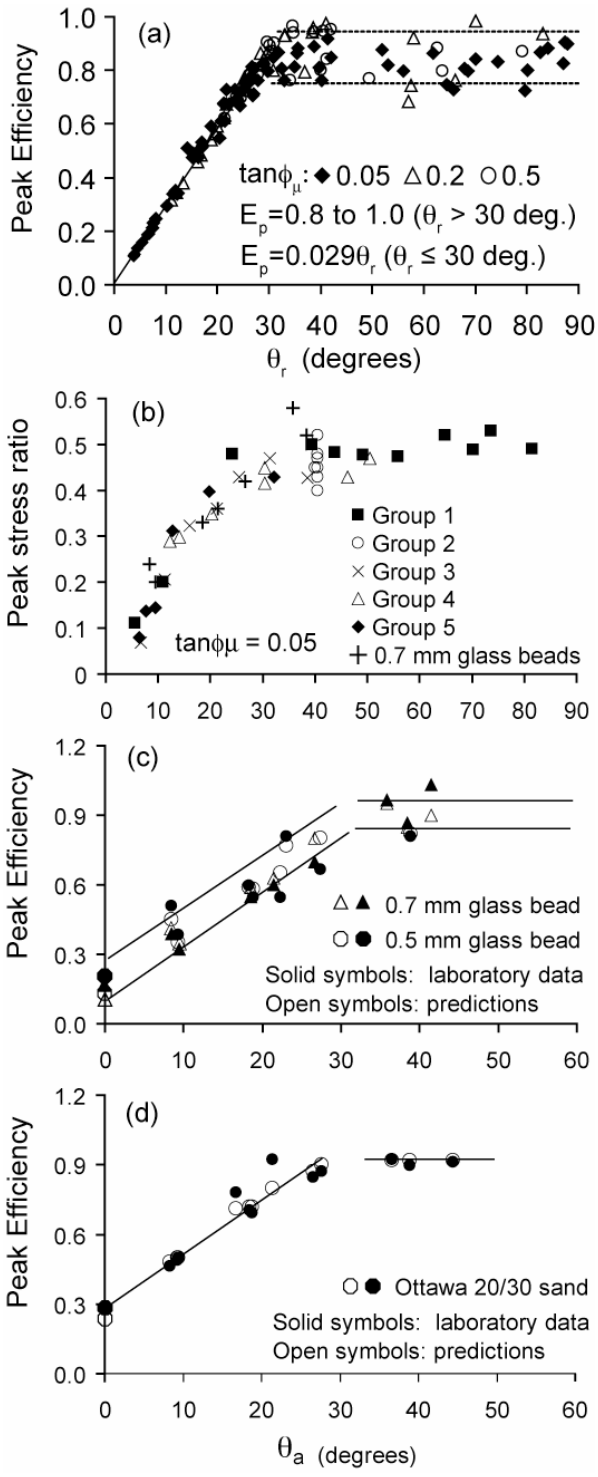

Figure 6.10. (a) Failure criterion in terms of efficiency and based on θ_r; (b) Laboratory data compared with all simulations with uniformly graded particles and $\tan\phi_\mu = 0.05$; (c) and (d) Predicted versus measured peak efficiency of glass beads ($\tan\phi_\mu = 0.1$) and Ottawa 20/30 sand ($\tan\phi_\mu = 0.2$). Profiles of surfaces used in laboratory tests and simulations are the same.